# Parallel electric fields in nonlinear magnetosonic waves

Seiichi Takahashi and Yukiharu Ohsawa[a)]
*Department of Physics, Nagoya University, Nagoya 464-8602, Japan*

(Received 20 September 2007; accepted 17 October 2007; published online 15 November 2007)

The electric field parallel to the magnetic field, $E_\parallel$, in nonlinear magnetosonic waves is studied theoretically and numerically. In the calculation of $E_\parallel$ based on the conventional reductive perturbation method, the terms related to the magnetic pressure cancel, and $E_\parallel$ is proportional to the electron temperature $T_e$. With a modified perturbation scheme assuming that the wave amplitude is in the range $(m_e/m_i)^{1/2}<\epsilon<1$, an expression for $E_\parallel$ is obtained that is proportional to the magnetic pressure in a cold plasma. Its integral along the magnetic field, $F=-\int E_\parallel ds$, is proportional to $\epsilon^2 m_i v_A^2$. One-dimensional, fully kinetic, electromagnetic particle simulations verify the theoretical predictions for small-amplitude waves. Further, they demonstrate that $eF$ becomes of the order of $\epsilon(m_i v_A^2+\Gamma_e T_e)$ in large-amplitude $[\epsilon\sim O(1)]$ oblique shock waves. These theory and simulations indicate that $E_\parallel$ in magnetosonic waves can be strong in a strong magnetic field. © *2007 American Institute of Physics*. [DOI: 10.1063/1.2806344]

## I. INTRODUCTION

In ideal (one-fluid) magnetohydrodynamics (MHD), perfect conductivity is assumed,

$$\boldsymbol{E}+\boldsymbol{v}\times\boldsymbol{B}/c=0, \tag{1}$$

where $\boldsymbol{E}$ is the electric field, $\boldsymbol{v}$ is the velocity, $\boldsymbol{B}$ is the magnetic field, and $c$ is the speed of light. Hence, the electric field parallel to the magnetic field is zero,

$$E_\parallel\equiv\boldsymbol{E}\cdot\boldsymbol{B}/B=0. \tag{2}$$

Parallel electric fields are thought to be quite weak in MHD phenomena in high temperature plasmas. Dissipation processes, such as magnetic reconnection and plasma heating, in the fluid with perfect conductivity have been a fundamental subject in plasma physics.[1–7]

In a two-fluid model, parallel electric fields appear even if there is no dissipation. Applying the reductive perturbation method[8,9] to nonlinear magnetosonic waves, one derives a Korteweg-de Vries (KdV) equation[10,11] and obtains the parallel electric field as

$$E_\parallel=-\frac{\Gamma_e T_e}{e}\frac{\partial}{\partial s}\left(\frac{n_1}{n_0}\right), \tag{3}$$

where $T_e$ is the electron temperature, $\Gamma_e$ is the specific heat ratio, $s$ is the length along the magnetic field, and $n_0$ and $n_1$ are the equilibrium and perturbed plasma densities, respectively.[11] Even though the magnetic and thermal pressures both contribute to the electric potential $\phi$ (and thus to the longitudinal electric field $-\nabla\phi$), the contribution of magnetic pressure to the parallel electric field disappears in the lowest-order calculation of $(\boldsymbol{E}\cdot\boldsymbol{B})/B$, and we have $E_\parallel$ that is proportional to $T_e$, as shown in Eq. (3). The parallel electric field is therefore weak compared with the longitudinal electric field. In particular, Eq. (3) predicts that $E_\parallel=0$ in the cold plasma limit $(T_e=T_i=0)$; the implication of this is not that $\boldsymbol{E}=0$ but that $\boldsymbol{E}$ is perpendicular to $\boldsymbol{B}$.

If we introduce the quantity $F$,

$$F=-\int E_\parallel ds, \tag{4}$$

Eq. (3) gives

$$eF=\Gamma_e T_e n_1/n_0, \tag{5}$$

which resembles the electric potential in an ion-acoustic wave. Equation (5) indicates that $eF\lesssim T_e$. The quantity $F$ is smaller than $\phi$; their difference is especially significant in low beta plasmas, where beta is the ratio of thermal to magnetic pressures.

The quantity $F$ has been used in theories of electron acceleration[6] and of positron acceleration[7] and has been examined with simulations in those papers. According to those simulations, $eF$ can far exceed thermal energy, $eF\gg T_e$. That is, $eF$ can become much greater than the prediction of the conventional perturbation theory, Eq. (5).[10,11]

This paper concerns $E_\parallel$ and $F$. In Sec. II, we apply a modified perturbation scheme[12] to nonlinear magnetosonic waves. This scheme has been originally developed to derive a nonlinear evolution equation in two-ion-species plasmas, in which there are two magnetosonic modes; i.e., the high- and low-frequency modes.[13–15] To focus on the high-frequency mode with $\omega\gtrsim\Omega_i$, where $\Omega_i$ is the ion gyrofrequency, this scheme assumes that the wave amplitudes $\epsilon$ are in the range $(m_e/m_i)^{1/2}<\epsilon<1$. Even though this paper discusses single-ion-species plasmas, we employ this scheme to analyze waves that have slightly greater amplitudes than those in the conventional scheme.[8–11] By using this method, we obtain new expressions for $E_\parallel$ and $F$ for quasiperpendicular $[\cos\theta\sim(m_e/m_i)^{1/2}]$ magnetosonic waves in a cold plasma, where $\theta$ is the angle between the external magnetic field and wave normal. In this theory, $F$ is proportional to $\epsilon^2 m_i v_A^2$, where $v_A$ is the Alfvén speed.

[a)]Author to whom correspondence should be addressed. Electronic mail: ohsawa@nagoya-u.jp.

 

In Sec. III, we test the two perturbation theories with one-dimensional (one space coordinate and three velocity components), fully kinetic, electromagnetic, particle simulations. We generate small-amplitude ($\epsilon<1$) magnetosonic solitary waves in the simulations and observe their field structures and strengths. It is found that in high beta plasmas, the values of $F$ measured in the simulations are consistent with the conventional theory. If the plasma beta is low ($T_e \ll m_i v_A^2$), however, the simulation values of $F$ are much greater than $F$ in the conventional theory and are much smaller than $\phi$. These are explained by the new perturbation theory. Further, we examine large-amplitude [$\epsilon \sim O(1)$], oblique [$\cos\theta \gg (m_e/m_i)^{1/2}$] shock waves, to which the above theories are inapplicable. Simulations show that $eF$ becomes of the order of $\epsilon(m_i v_A^2 + \Gamma_e T_e)$. Even if $T_e \ll m_i v_A^2$, $F$ can become of the same order of magnitude as $\phi$ in shock waves, although $F$ remains to be smaller than $\phi$.

In Sec. IV, we summarize our work and mention some subjects that should be studied in the future. The present results indicate that strong parallel electric fields can be created in MHD phenomena in strong magnetic fields, such as those in coronal magnetic tubes and around pulsars.[16–20]

## II. PARALLEL ELECTRIC FIELD

### A. Potential and parallel electric field in the conventional perturbation scheme

We consider magnetosonic waves propagating in the $x$ direction in an external magnetic field $\boldsymbol{B}_0 = B_0(\cos\theta, 0, \sin\theta) = (B_{x0}, 0, B_{z0})$. In the conventional reductive perturbation method[8,9] to derive the KdV equation,[10,11] the magnetic perturbation $B_{z1}$ is related to $n_1$ as

$$\frac{B_{z1}}{B_0} = \frac{(v_{p0}^2 - c_s^2)}{v_A^2 \sin\theta} \frac{n_1}{n_0}, \tag{6}$$

and, by use of $B_{z1}$, the perturbation of electric potential is expressed as

$$e\phi_1 = m_i \left[ \frac{(\Omega_e + \Omega_i)(v_{p0}^2 - c_s^2) v_{p0}^2}{\Omega_e (v_{p0}^2 - v_A^2 \cos^2\theta)} + \frac{\Gamma_e p_{e0}}{n_0 (m_i + m_e)} - \frac{m_e \Gamma_i p_{i0}}{m_i n_0 (m_i + m_e)} \right] \frac{v_A^2 \sin\theta}{(v_{p0}^2 - c_s^2)} \frac{B_{z1}}{B_0}, \tag{7}$$

where $c_s$ is the sound speed, $\Omega_j$ ($j=e$ or $i$) is the gyrofrequency ($\Omega_e<0$), $\Gamma_j$ is the specific heat ratio, and $p_{j0}$ is the equilibrium thermal pressure.[11] The quantity $v_{p0}$ is the propagation speed of the fast magnetosonic wave in the long-wavelength limit,

$$v_{p0}^2 = (1/2)\{(v_A^2 + c_s^2) + [(v_A^2 + c_s^2)^2 - 4 v_A^2 c_s^2 \cos\theta]^{1/2}\}. \tag{8}$$

The first term on the right-hand side of Eq. (7) is mainly due to magnetic pressure, while the second and third terms are due to thermal pressure; the third term is $\sim m_e/m_i$ times as small as the second one. Equation (7) reduces to

$$e\phi_1 \simeq m_i \left[ v_A^2 + \frac{\Gamma_e p_{e0}}{n_0 (m_i + m_e)} \right] \frac{B_{z1}}{B_0}, \tag{9}$$

in quasiperpendicular waves with $\sin\theta \simeq 1$.

The electric fields $E_{x1}$ and $E_{z1}$ are given as

$$\frac{E_{x1}}{B_0} = -\frac{v_A^2 \sin\theta}{\Omega_i \Omega_e c} \left[ \frac{(\Omega_e + \Omega_i) v_{p0}^2}{(v_{p0}^2 - v_A^2 \cos^2\theta)} + \frac{c_s^2 (\Omega_e \Gamma_e p_{e0} + \Omega_i \Gamma_i p_{i0})}{(v_{p0}^2 - c_s^2)(\Gamma_e p_{e0} + \Gamma_i p_{i0})} \right] \frac{\partial}{\partial \xi} \frac{B_{z1}}{B_0}, \tag{10}$$

$$\frac{E_{z1}}{B_0} = \frac{(\Omega_e + \Omega_i) v_{p0}^2 v_A^2 \cos\theta}{\Omega_i \Omega_e c (v_{p0}^2 - v_A^2 \cos^2\theta)} \frac{\partial}{\partial \xi} \frac{B_{z1}}{B_0}. \tag{11}$$

The first term on the right-hand side of Eq. (10) and the field $E_{z1}$ are mainly due to magnetic pressure. These terms cancel in the lowest order calculation of $E_\parallel$,

$$E_{\parallel 1} = E_{x1} \cos\theta + E_{z1} \sin\theta, \tag{12}$$

and we have Eq. (3), which is proportional to the electron temperature.

For one-dimensional waves ($\partial/\partial y = \partial/\partial z = 0$), one can write the integral of $E_\parallel$ along the magnetic field $\boldsymbol{B}$ as

$$F = -\int E_\parallel ds = -\int \frac{(\boldsymbol{E}\cdot\boldsymbol{B})}{B_{x0}} dx, \tag{13}$$

where we have used the relation $ds/B = dx/B_{x0}$. The conventional perturbation scheme gives $F$ that is proportional to $T_e$, as shown by Eq. (5).

### B. Calculation based on another ordering

As can be seen from Eq. (7), the mass ratio $m_e/m_i$ is treated as order unity in the above perturbation scheme. This suggests that the amplitude $\epsilon$, which is used as the smallness parameter in the expansion, must be smaller than $m_e/m_i$.

Instead of the conventional ordering, we now adopt the ordering used for the wave theory for two-ion-species plasmas;[12] i.e., we assume that the wave amplitudes are in the range

$$\eta < \epsilon < 1, \tag{14}$$

where

$$\eta = (m_e/m_i)^{1/2}. \tag{15}$$

We introduce stretched coordinates,

$$\xi = \epsilon^{1/2}(x - v_A t), \tag{16}$$

$$\tau = \epsilon^{3/2} t, \tag{17}$$

and expand plasma variables as

$$B_z = B_0 \sin\theta + \epsilon B_{z1} + \epsilon^2 B_{z2} + \cdots, \tag{18}$$

$$E_y = \epsilon E_{y1} + \epsilon^2 E_{y2} + \cdots, \tag{19}$$

$$v_{jx} = \epsilon v_{jx1} + \epsilon^2 v_{jx2} + \cdots, \tag{20}$$

$$v_{jz} = \eta^{-1}(\epsilon^2 v_{jz1} + \epsilon^3 v_{jz2} + \cdots), \tag{21}$$

$$n_j = n_{j0} + \epsilon n_{j1} + \epsilon^2 n_{j2} + \cdots, \tag{22}$$

and

$$B_y = \epsilon^{3/2} B_{y1} + \epsilon^{5/2} B_{y2} + \cdots, \tag{23}$$

$$E_x = \eta^{-1}(\epsilon^{3/2} E_{x1} + \epsilon^{5/2} E_{x2} + \cdots), \tag{24}$$

$$E_z = \epsilon^{3/2} E_{z1} + \epsilon^{5/2} E_{z2} + \cdots, \tag{25}$$

$$v_{jy} = \eta^{-1}(\epsilon^{3/2} v_{jy1} + \epsilon^{5/2} v_{jy2} + \cdots). \tag{26}$$

Because $\nabla \cdot \boldsymbol{B} = 0$, $B_x$ is constant. Further, we assume that $\cos\theta \sim O(\eta)$. Then, after some algebra, we obtain a KdV equation,

$$\frac{\partial B_{z1}}{\partial \tau} + \frac{3 v_A}{2} \frac{B_{z1}}{B_0} \frac{\partial B_{z1}}{\partial \xi} + \frac{c^2 v_A}{2\omega_{pe}^2} \left(1 - \frac{\cos^2\theta}{\eta^2}\right) \frac{\partial^3 B_{z1}}{\partial \xi^3} = 0, \tag{27}$$

where $\omega_{pe}$ is the electron plasma frequency (for the details of the calculation, see the Appendix). Here, for simplicity, we have considered a cold plasma.

The parallel electric field including up to the second-order terms is given as

$$E_\parallel = \frac{\boldsymbol{E}\cdot\boldsymbol{B}}{B} = \frac{\boldsymbol{E}_1 \cdot \boldsymbol{B}_0}{B_0}\left(1 - \frac{\boldsymbol{B}_1 \cdot \boldsymbol{B}_0}{B_0^2}\right) + \frac{\boldsymbol{E}_1 \cdot \boldsymbol{B}_1}{B_0} + \frac{\boldsymbol{E}_2 \cdot \boldsymbol{B}_0}{B_0}. \tag{28}$$

Inspection of Eqs. (A17), (A18), and (A20) in the Appendix shows that the term $\boldsymbol{E}_1 \cdot \boldsymbol{B}_1 = E_{y1} B_{y1} + E_{z1} B_{z1}$ vanishes; this is also the case with the conventional theory for finite beta plasmas. Further, the term $\boldsymbol{E}_1 \cdot \boldsymbol{B}_0 / B_0 = E_{x1} \cos\theta/\eta + E_{z1} \sin\theta$ is zero in cold plasmas. With the aid of the second-lowest order equation of Eqs. (A11) and (A25) in the Appendix, one can express $\boldsymbol{E}_2 \cdot \boldsymbol{B}_0 / B_0$ with lowest-order variables. We thus find $E_\parallel$ and $F$ in the present perturbation scheme as

$$E_\parallel = E_{x2} \frac{\cos\theta}{\eta} + E_{z2} \sin\theta = \frac{m_i v_A^2}{e} \cos\theta \left(\frac{c}{\omega_{pe}}\right)^2 \frac{\partial^3}{\partial \xi^3} \frac{B_{z1}}{B_0}, \tag{29}$$

$$eF = -m_i v_A^2 \left(\frac{c}{\omega_{pe}}\right)^2 \frac{\partial^2}{\partial \xi^2} \frac{B_{z1}}{B_0}, \tag{30}$$

where we have used the approximation $\sin\theta \simeq 1$ [accurate up to the first order of $(\pi/2 - \theta)$] in the final expressions. The two quantities are proportional to $B_0^2$ for a fixed normalized amplitude $B_{z1}/B_0$. The fact that $F$ is proportional to $\partial^2 B_{z1}/\partial \xi^2$ indicates that $F$ has a profile different from $B_{z1}$. [In the conventional theory, they have similar profiles, as shown by Eq. (5).] Further, because $\partial^2/\partial\xi^2 \sim \epsilon$ in the perturbation scheme, $F$ in Eq. (30) is of the order of $\epsilon^2$.

In Fig. 1, we plot the magnitude of $F$ in the solitary wave as a function of the amplitude $B_{z1}/B_0$ for $|\Omega_e|/\omega_{pe} = 1.0$ and 0.01, where $F_T$ (dotted line) and $F_B$ (solid line), respectively, represent $F$ given by the conventional theory (5) and by the new one, Eq. (30). Here, we have taken the electron temperature and propagation angle to be $T_e = 10$ eV and $\theta = 85°$ (the critical angle $\theta_c$ at which $\cos\theta_c = \eta$ is 88.7° for $m_i/m_e = 1836$[10,11]). For this temperature, $F_B$ is rather small at $|\Omega_e|/\omega_{pe} = 0.01$ compared to $F_T$ (bottom panel). At $|\Omega_e|/\omega_{pe} = 1.0$ (top panel), however, $F_B$ far exceeds $F_T$ even

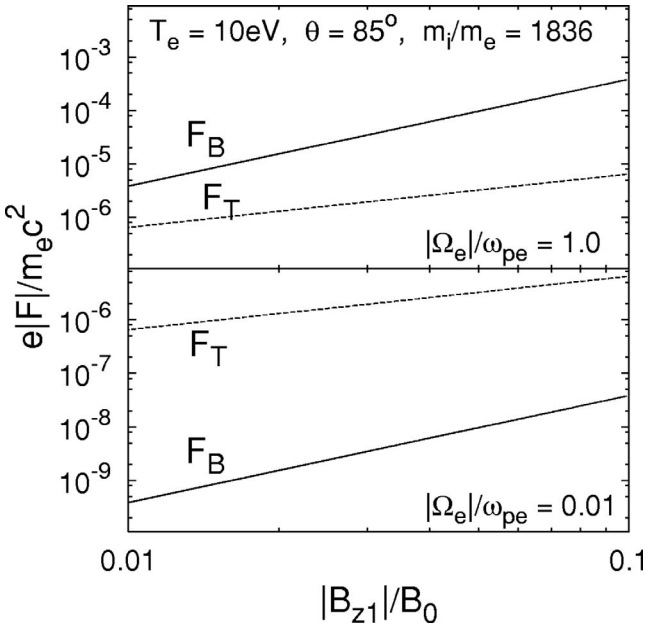


FIG. 1. Magnitude of $F$ vs amplitude. When the magnetic field is strong, $F_B$ exceeds $F_T$.

for the amplitudes $(B_{z1}/B_0) \lesssim (m_e/m_i)^{1/2}$. As mentioned above, $F_B$ and $F_T$ are proportional to $(B_{z1}/B_0)^2$ and $(B_{z1}/B_0)$, respectively.

Here, we have estimated the right-hand side of Eq. (30) as follows: We move to the wave frame of a stationary solitary wave, where the fields depend only on $X = \xi - \lambda\tau$; $\lambda$ is related to the wave amplitude as $\lambda = (v_A/2)(B_{z1}/B_0)$.[8–11] We rewrite Eq. (27) using $X$ and integrate it to obtain

$$\frac{d^2}{dX^2} \frac{B_{z1}}{B_0} = \frac{2[\lambda B_{z1}/B_0 - (3v_A/4)(B_{z1}/B_0)^2]}{v_A (c/\omega_{pe})^2 (1 - \cos^2\theta/\eta^2)}. \tag{31}$$

Then, we may express the peak value of $F$ as

$$\frac{eF}{m_i v_A^2} = \frac{1}{2}\left(1 - \frac{\cos^2\theta}{\eta^2}\right)^{-1} \left(\frac{B_{z1}}{B_0}\right)^2. \tag{32}$$

Figure 2 shows the ratio $F_B/F_T$ as a function of $|\Omega_e|/\omega_{pe}$ for $T_e = 10$ eV, 100 eV, and 1000 eV; the propagation angle and amplitude are $\theta = 85°$ and $B_{z1}/B_0 = 0.1$. For $T_e = 10$ eV, $F_B/F_T$ exceeds unity for $|\Omega_e|/\omega_{pe} \gtrsim 0.1$.

If we take the cold plasma limit, $T_e = T_i = 0$, in the conventional theory and calculate $E_\parallel$ up to the second order, we also obtain an expression for $E_\parallel$ similar to Eq. (29). However, this scheme does not give proper profiles for some quantities for $\epsilon \gtrsim (m_e/m_i)^{1/2}$. This will be discussed again in the next section.

## III. NUMERICAL EXPERIMENTS

### A. Simulation model and parameters

In this section, we investigate the parallel electric field with a one-dimensional (one space coordinate and three velocities), relativistic, electromagnetic particle simulation code with full ion and electron dynamics,[21] by observing the propagation of nonlinear magnetosonic waves. As the initial wave profiles in the simulations, we use the solitary wave

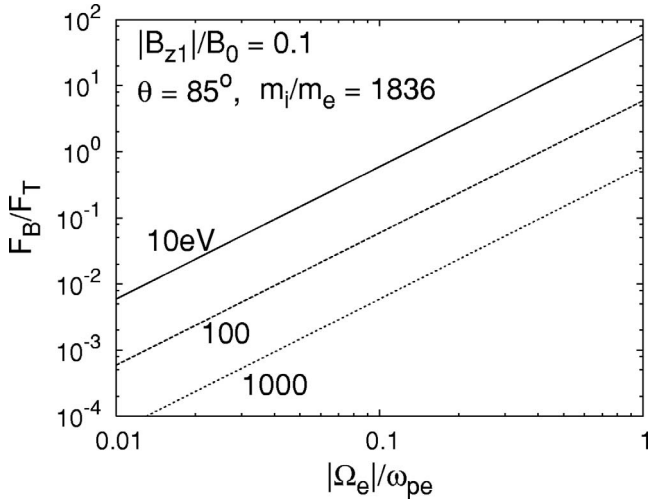


FIG. 2. Ratio $F_B/F_T$ as a function of $|\Omega_e|/\omega_{pe}$. The cases with $T_e=10$ eV, 100 eV, and 1000 eV are shown.

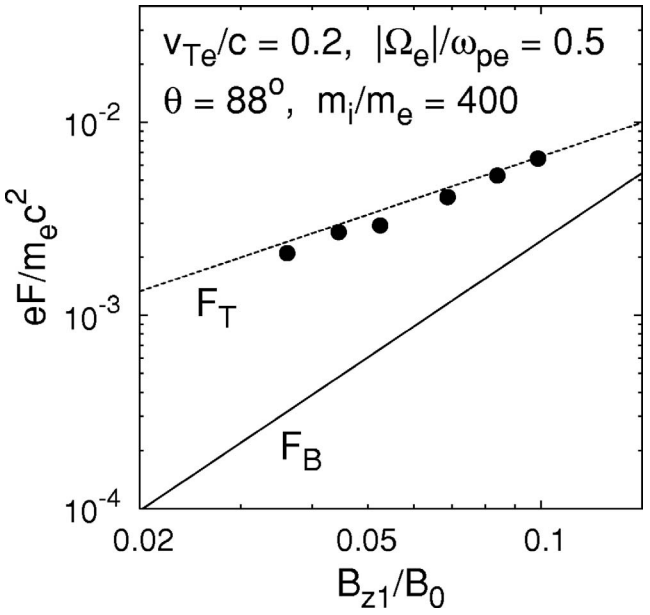


FIG. 3. Magnitude of $F$ as a function of the amplitude. The dots show simulation results. The electron temperature is rather high, and the simulation results are explained by the conventional theory $F_T$.

solutions of the KdV equation (27). Specifically, we initially give the perturbations of $B_y$, $B_z$, $E_y$, $E_z$, densities, and velocities according to Eqs. (A17)–(A21). Because we take $n_i$ and $n_e$ to be exactly the same at $t=0$, the longitudinal electric field $E_x$ is initially zero. In a self-consistent simulation, however, $E_x$ is created in the evolution of the wave. The profiles of other fields including $E_\parallel$ are also adjusted to their most stable forms. After the pulse propagation has become stationary, we measure the field strengths. The field profiles measured in this way are insensitive to their initial profiles; even if we use the solitary wave solutions obtained from the conventional theory, we have similar results.

The simulation parameters are as follows: The system size is $L=2048\Delta_g$, where $\Delta_g$ is the grid spacing. The numbers of simulation particles are $N_i=N_e\simeq 2.5\times 10^6$. The ion-to-electron mass ratio is $m_i/m_e=400$; hence, the critical angle is $\theta_c=87.1°$. The speed of light is $c/(\omega_{pe}\Delta_g)=10$. The ion thermal speed is fixed to be $(T_i/m_i)^{1/2}/(\omega_{pe}\Delta_g)=0.013$. The time step is $\omega_{pe}\Delta t=0.05$.

### B. Simulation study of *F*

First, we confirm that if the electron temperature is high, simulations give results consistent with the conventional theory. In Fig. 3, we plot the magnitude of $F$ as a function of the pulse amplitude $B_{z1}/B_0$, where the closed circles, dashed line, and thin solid line, respectively, represent the simulation result, conventional theory ($F_T$), and new theory ($F_B$). Here, the propagation angle is $\theta=88°$, the electron thermal velocity is $v_{Te}/(\omega_{pe}\Delta_g)=2.0$, and the strength of the external magnetic field is $|\Omega_e|/\omega_{pe}=0.5$, which gives the Alfvén speed as $v_A/(\omega_{pe}\Delta_g)=0.25$. For the present parameters, $F_B$ is much smaller than $F_T$, which in fact is natural because the effect of $T_e$ is not included in $F_B$. The simulation results are close to $F_T$.

Next, we examine the case with a lower $T_e$ $[v_{Te}/(\omega_{pe}\Delta_g)=0.26]$ and a higher $B_0$ $(|\Omega_e|/\omega_{pe}=1.0)$ [hence, $v_A/(\omega_{pe}\Delta_g)=0.5$ and $m_ec^2=m_iv_A^2$], with other parameters kept unchanged. As shown in Fig. 4, $F_T$ is much smaller than $F_B$ in this case, and the simulation results agree with $F_B$ much better than with $F_T$.

Figure 5 compares the profiles of $\phi$ (dotted line) and $F$ (solid line) for the amplitude $B_{z1}/B_0=0.057$. This figure shows two important features of $F$. First, $F$ is much smaller than $\phi$; the ratio of their peak values is $F/\phi\simeq 0.04$ in this case. Second, $F$ has dips on both sides of the pulse, although $\phi$ has a typical profile of KdV solitons. This is accounted for by Eq. (30), which shows that $F$ is proportional to $\partial^2\phi/\partial x^2$ ($\phi$ and $B_{z1}$ have similar profiles).

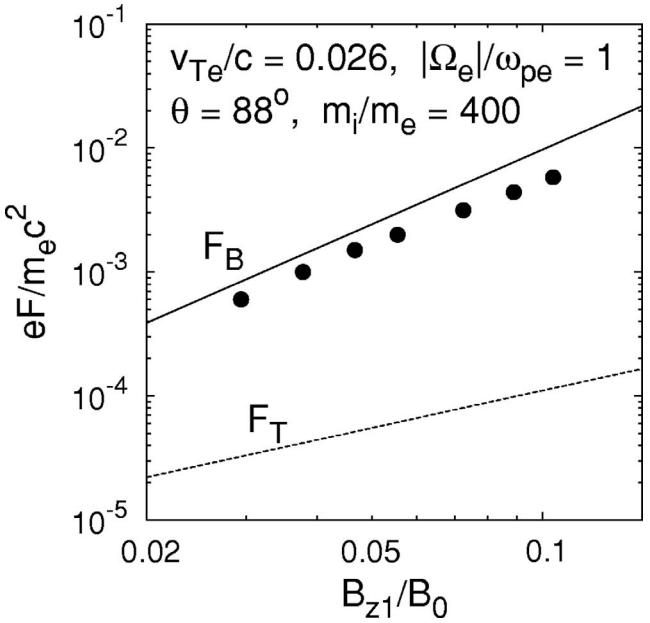


FIG. 4. $F$ vs amplitude. Here, $|\Omega_e|/\omega_{pe}$ is higher, and $v_{Te}$ is lower than those in Fig. 3.

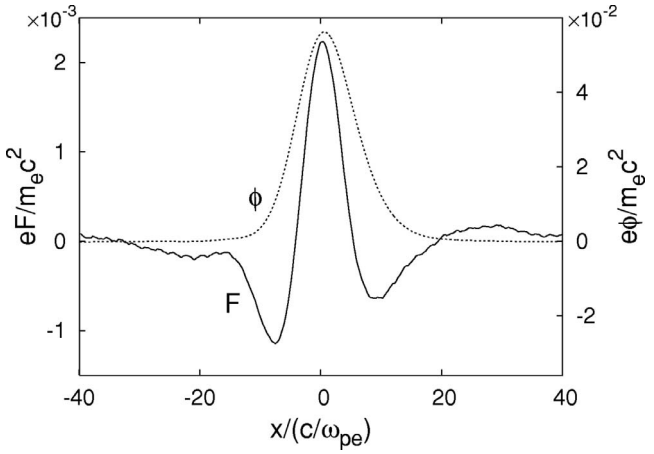


FIG. 5. Profiles of $F$ and $\phi$ observed in a simulation.

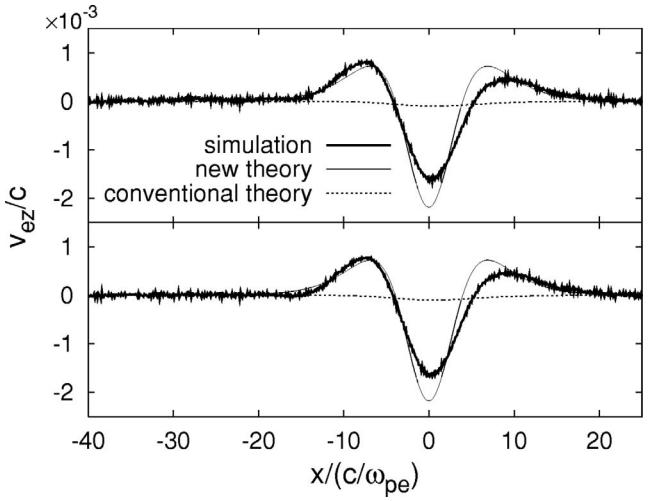


FIG. 6. Profiles of $v_{ez}$ obtained by simulations (thick solid lines), new theory (thin solid lines), and conventional theory (dotted lines). The initial profiles were given according to the new theory in the upper panel and the conventional theory in the lower panel. After the wave propagation has become stationary in the simulation, $v_{ez}$ has a profile close to that given by the new theory in both the upper and lower panels.

Because $F$ is much smaller than $\phi$, $F$ is easily masked by thermal noise. We have measured the amplitude and profile of $F$ as follows: We carry out a simulation for solitary wave propagation to take the data of $\boldsymbol{E}$ and $\boldsymbol{B}$. From the profiles of $B_z(x,t_j)$ at consecutive times $t_j$ $(j=1,2,\ldots,N)$, we obtain the trajectory and propagation speed $v_{\rm sh}$ of the pulse. We then average the profiles of $F(x-v_{\rm sh}t_j,t_j)$ over time,

$$\langle F\rangle = \frac{1}{N}\sum_{j=1}^{N} F(x-v_{\rm sh}t_j,t_j). \tag{33}$$

With this procedure, thermal fluctuations are smoothed out, and the profile of $F$ appears.

Even in the cold plasma limit $(T_e=T_i=0)$, the profiles of some quantities in the conventional theory are different from those in the new theory. For instance, $v_{ez}$ is given by Eq. (A19) in the new theory and by a different equation,

$$v_{ez} = -v_A\cos\theta\frac{B_{z1}}{B_0}, \tag{34}$$

in the conventional theory. Figure 6 shows the profiles of $v_{ez}$ obtained by simulations (thick solid lines), new theory (thin solid lines), and conventional theory (dotted lines); in the simulations, the initial field profiles were given by Eqs. (A17)–(A21) in the upper panel and by the conventional theory in the lower panel. (The simulation parameters are the same as those in Fig. 4.) Even though the initial profiles are different, the two $v_{ez}$ profiles formed in the simulations are quite similar. Clearly, the simulation results fit much better to the new theory than to the conventional theory in both the upper and lower panels.

In Fig. 7, we show the case of $\theta=86°$ (other parameters are the same as those in Fig. 4). This angle is smaller than $\theta_c$, and the KdV equation gives rarefactive solitons.[10,11] However, the above discussion also applies to this case. That is, if $T_e$ is low, $F_B$ exceeds $F_T$, and the simulation results are closer to $F_B$.

To this point, we have restricted ourselves to small-amplitude $(\epsilon\ll 1)$, quasiperpendicular $(\cos\theta\sim\eta)$ waves. Finally, we examine $F$ in large-amplitude $(\epsilon\gtrsim 1)$, oblique $(\cos\theta\gg\eta)$ shock waves, which is covered by neither the conventional nor present perturbation theories. Figure 8 shows the values of $F$ (closed circles and triangles) and $\phi$ (open circles and triangles) formed in shock waves at $\theta=60°$ with the amplitudes $2\lesssim B_{z1}/B_0\lesssim 10$ for $|\Omega_e|/\omega_{pe}=1.0$ (circles) and 0.5 (triangles); since their propagation speeds are higher than the pulse speeds in Figs. 4 and 7, we have chosen a longer system length, $L=8192\Delta_g$. The electron temperature is the same as those in Figs. 4 and 7, and thus $T_e=m_ev_{Te}^2\ll m_iv_A^2$. The dotted line represents $|F_B|$, which we have drawn by merely extrapolating Eq. (32) to a larger amplitude and smaller angle regime, while the solid line represents a phenomenological relation expressed by

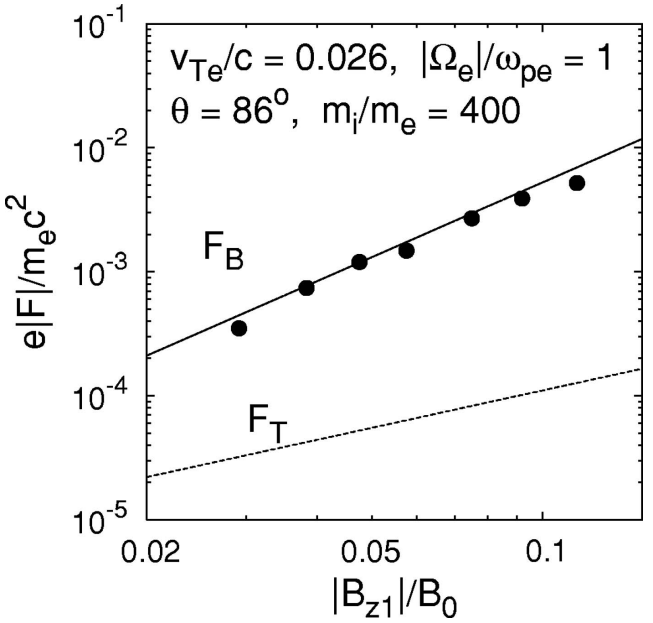


FIG. 7. $F$ vs amplitude. The propagation angle is taken to be $\theta=86°$, which is smaller than $\theta_c$, with other parameters being the same as those in Fig. 4.

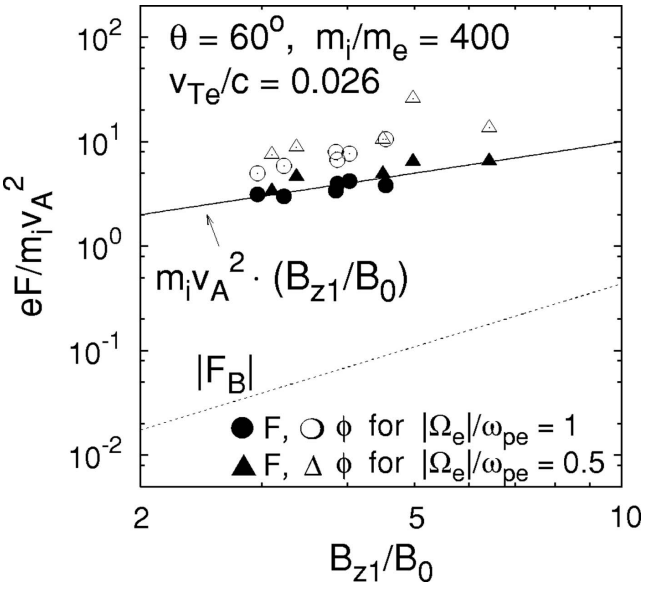


FIG. 8. Magnitudes of $F$ and $\phi$ in shock waves at $\theta=60°$. The closed circles and triangles represent simulation results for $F$. The solid line is a phenomenological expression $F=\epsilon m_i v_A^2$. The open circles and triangles represent $\phi$.

$$eF \sim m_i v_A^2 \frac{B_{z1}}{B_0}. \tag{35}$$

It is found that $F$ is always smaller than $\phi$, although their ratios, $F/\phi$, are greater than those in the small-amplitude case. Further, the simulation values of $F$ fit to the phenomenological line fairly well, much better than to the extrapolated $|F_B|$.

Figure 9 shows the case of higher electron beta; $v_{Te}/c=0.2$, and hence $T_e=m_i v_A^2$ for $|\Omega_e|/\omega_{pe}=0.2$. The solid line represents a phenomenological relation including the effect of $T_e$,

$$eF \sim (m_i v_A^2 + \Gamma_e T_e)\frac{B_{z1}}{B_0}. \tag{36}$$

We see that the values of $eF$ observed in the simulations are of the same order of magnitude as those given by Eq. (36) when $T_e \sim m_i v_A^2$. One can use Eq. (36) for the estimate of $eF$ for both low and high beta cases.

At present we do not have a mathematical theory for $F$ in large-amplitude waves. One can obtain Eq. (35) by simply setting $\partial/\partial\xi \sim (c/\omega_{pe})^{-1}$ in Eq. (30) and obtain Eq. (36) by adding the effect of $T_e$ to Eq. (35). Nevertheless, these procedures are not mathematically rigorous, because Eq. (30) is for small-amplitude, quasiperpendicular waves. An attempt should be made in the future to theoretically obtain $F$ in large-amplitude waves in a self-consistent manner.

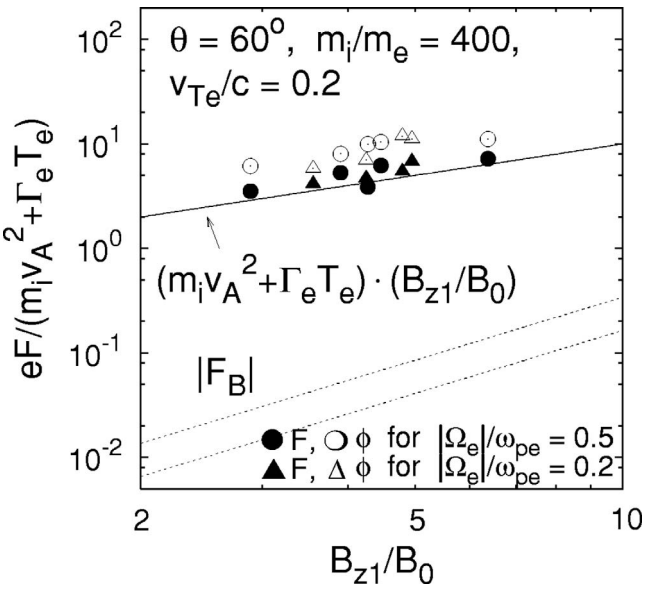


FIG. 9. Magnitudes of $F$ and $\phi$ in shock waves at $\theta=60°$. The electron thermal speed is higher than that in Fig. 8, and the magnetic fields are weaker. The solid line represents a phenomenological expression $F=\epsilon(m_i v_A^2+\Gamma_e T_e)$. The upper and lower dotted lines show extrapolated $|F_B|$ for $|\Omega_e|/\omega_{pe}=0.5$ and 0.2, respectively.

## IV. SUMMARY

We have studied the parallel electric field $E_\parallel$ and $F$ $(=-\int E_\parallel ds)$ in nonlinear magnetosonic waves. In the conventional perturbation theory, they are proportional to the electron temperature. In the present paper, we have applied a modified perturbation scheme, which assumes that $(m_e/m_i)^{1/2}<\epsilon<1$, to quasiperpendicular waves in a cold, single-ion-species plasma and obtained expressions for $E_\parallel$ and $F$ that are proportional to the magnetic pressure. When the plasma beta value is high, $F_T$ ($F$ in the conventional theory) is greater than $F_B$ ($F$ in the new theory), while in low beta plasmas, $F_B$ exceeds $F_T$. With one-dimensional, fully kinetic, relativistic, electromagnetic particle simulations, we then have examined the field profiles and strengths in small-amplitude, quasiperpendicular magnetosonic solitary waves and verified the theoretical predictions. Further, we have numerically investigated large-amplitude $[\epsilon \sim O(1)]$ shock waves propagating obliquely to an external magnetic field with $\cos\theta \gg (m_e/m_i)^{1/2}$ for the cases with $T_e \ll m_i v_A^2$ and with $T_e \sim m_i v_A^2$. The simulation values are approximately expressed by $eF \sim \epsilon(m_i v_A^2+\Gamma_e T_e)$. In large-amplitude waves, $F$ and $\phi$ are of the same order of magnitude, with $F<\phi$, in both low and high beta plasmas, which in fact differs from the small-amplitude case in which $F \ll \phi$ in low beta plasmas.

Although the magnetosonic wave is one of the main MHD waves, its $E_\parallel$ can become quite strong in a strong magnetic field. This result should be important in many plasmas; for instance, in coronal magnetic tubes and around pulsars.

The theory in this paper was mainly concerned with small-amplitude waves. It would be desirable to extend the theory to large-amplitude waves so that we can estimate $F$ in a shock wave in a self-consistent manner. In addition, in view of the fact that in large-amplitude magnetosonic waves, relativistic effects become significant even in fluid motions if $|\Omega_e|/\omega_{pe}>1$,[22] it should also be important to develop a relativistic theory.

## ACKNOWLEDGMENTS

This work was carried out by the joint research program of the Solar-Terrestrial Environment Laboratory, Nagoya University, and by the collaboration program, NIFS06KTAT017, of the National Institute for Fusion Science.

## APPENDIX: DERIVATION OF NONLINEAR EVOLUTION EQUATION

Here, we derive the KdV equation for quasiperpendicular magnetosonic waves with amplitudes $(m_e/m_i)^{1/2}<\epsilon<1$ in a cold plasma. We normalize the length, time, and velocity to $c/\omega_{pe}$, $(c/\omega_{pe})/v_A$, and $v_A$, respectively, and the magnetic field, electric field, density, and charge to $B_0$, $B_0v_A/c$, $n_0$, and $e$, respectively. Then, the two-fluid model may be written as

$$\frac{\partial n_j}{\partial t}+\nabla\cdot(n_j\boldsymbol{v}_j)=0, \tag{A1}$$

$$\left[\frac{\partial}{\partial t}+(\boldsymbol{v}_j\cdot\nabla)\right]\boldsymbol{v}_j=\frac{\Omega_j}{|\Omega_e|}\frac{1}{\eta}(\boldsymbol{E}+\boldsymbol{v}_j\times\boldsymbol{B}), \tag{A2}$$

$$\frac{\partial\boldsymbol{B}}{\partial t}=-\nabla\times\boldsymbol{E}, \tag{A3}$$

$$\nabla\times\boldsymbol{B}=\eta\sum_j n_jq_j\boldsymbol{v}_j, \tag{A4}$$

where the subscript $j$ refers to the ions $(j=i)$ or electrons $(j=e)$. We apply the perturbation scheme (16)–(26) to the above set of equations under the assumption that $\cos\theta\sim O(\eta)$ and $\sin\theta\simeq 1$, which is accurate to within the first order of $(\pi/2-\theta)$. Then, from the continuity equation we have

$$\epsilon^{3/2}\left(-\frac{\partial n_{j1}}{\partial\xi}+n_{j0}\frac{\partial v_{jx1}}{\partial\xi}\right)+\epsilon^{5/2}\left(-\frac{\partial n_{j2}}{\partial\xi}+\frac{\partial n_{j1}}{\partial\tau}+n_{j0}\frac{\partial v_{jx2}}{\partial\xi}+\frac{\partial n_{j1}v_{jx1}}{\partial\xi}\right)+\cdots=0. \tag{A5}$$

We obtain the $x$, $y$, and $z$ components of the momentum equation for the ions as

$$\epsilon^{3/2}\left[\frac{\partial v_{ix1}}{\partial\xi}+(E_{x1}+v_{iy1})\right]+\epsilon^{5/2}\left[\frac{\partial v_{ix2}}{\partial\xi}-\frac{\partial v_{ix1}}{\partial\tau}-v_{ix1}\frac{\partial v_{ix1}}{\partial\xi}+(E_{x2}+v_{iy2}+v_{iy1}B_{z1})\right]+\cdots=0, \tag{A6}$$

$$\eta^{-1}\epsilon^2\frac{\partial v_{iy1}}{\partial\xi}+\eta^{-1}\epsilon^3\left(\frac{\partial v_{iy2}}{\partial\xi}-\frac{\partial v_{iy1}}{\partial\tau}-v_{ix1}\frac{\partial v_{iy1}}{\partial\xi}\right)+\cdots=0, \tag{A7}$$

$$\eta^{-1}\epsilon^{5/2}\frac{\partial v_{iz1}}{\partial\xi}+\eta^{-1}\epsilon^{7/2}\left(\frac{\partial v_{iz2}}{\partial\xi}-\frac{\partial v_{iz1}}{\partial\tau}-v_{ix1}\frac{\partial v_{iz1}}{\partial\xi}\right)+\cdots=0, \tag{A8}$$

and those for the electrons as

$$\eta^{-2}\epsilon^{3/2}(E_{x1}+v_{ey1})+\eta^{-2}\epsilon^{5/2}(E_{x2}+v_{ey2}+v_{ey1}B_{z1})+\cdots=0, \tag{A9}$$

$$\eta^{-1}\epsilon(E_{y1}-v_{ex1})+\eta^{-1}\epsilon^2\left(-\frac{\partial v_{ey1}}{\partial\xi}+E_{y2}+\frac{\cos\theta}{\eta}v_{ez1}-v_{ex2}-v_{ex1}B_{z1}\right)+\cdots=0, \tag{A10}$$

$$\eta^{-1}\epsilon^{3/2}\left(E_{z1}-\frac{\cos\theta}{\eta}v_{ey1}\right)+\eta^{-1}\epsilon^{5/2}\left(-\frac{\partial v_{ez1}}{\partial\xi}+E_{z2}+v_{ex1}B_{y1}-\frac{\cos\theta}{\eta}v_{ey2}\right)+\cdots=0. \tag{A11}$$

The $y$ and $z$ components of Faraday's law read as

$$\epsilon^2\left(-\frac{\partial B_{y1}}{\partial\xi}-\frac{\partial E_{z1}}{\partial\xi}\right)+\epsilon^3\left(-\frac{\partial B_{y2}}{\partial\xi}+\frac{\partial B_{y1}}{\partial\tau}-\frac{\partial E_{z2}}{\partial\xi}\right)+\cdots=0, \tag{A12}$$

$$\epsilon^{3/2}\left(-\frac{\partial B_{z1}}{\partial\xi}+\frac{\partial E_{y1}}{\partial\xi}\right)+\epsilon^{5/2}\left(-\frac{\partial B_{z2}}{\partial\xi}+\frac{\partial B_{z1}}{\partial\tau}+\frac{\partial E_{y2}}{\partial\xi}\right)+\cdots=0. \tag{A13}$$

The $x$, $y$, and $z$ components of Ampére's law become

$$\epsilon\sum_j n_{j0}q_jv_{jx1}+\epsilon^2\left(\sum_j n_{j0}q_jv_{jx2}+\sum_j n_{j1}q_jv_{jx1}\right)+\cdots=0, \tag{A14}$$

$$\epsilon^{3/2}\left(\frac{\partial B_{z1}}{\partial\xi}+\sum_j n_{j0}q_jv_{jy1}\right)+\epsilon^{5/2}\left(\frac{\partial B_{z2}}{\partial\xi}+\sum_j n_{j0}q_jv_{jy2}+\sum_j n_{j1}q_jv_{jy1}\right)+\cdots=0, \tag{A15}$$

$$\epsilon^2\left(\frac{\partial B_{y1}}{\partial\xi}-\sum_j n_{j0}q_jv_{jz1}\right)+\epsilon^3\left(\frac{\partial B_{y2}}{\partial\xi}-\sum_j n_{j0}q_jv_{jz2}-\sum_j n_{j1}q_jv_{jz1}\right)+\cdots=0. \tag{A16}$$

From the lowest-order equations, we obtain the relations among the quantities with the subscript 1 as

$$n_{e1}=n_{i1}=v_{ex1}=v_{ix1}=E_{y1}=B_{z1}, \tag{A17}$$

$$v_{ey1}=-E_{x1}=\frac{\partial B_{z1}}{\partial\xi}, \tag{A18}$$

$$v_{ez1}=\frac{\cos\theta}{\eta}\frac{\partial^2B_{z1}}{\partial\xi^2}, \tag{A19}$$

$$v_{iy1}=v_{iz1}=0, \tag{A20}$$

$$E_{z1} = -B_{y1} = \frac{\cos\theta}{\eta}\frac{\partial B_{z1}}{\partial \xi}. \tag{A21}$$

Combining Eqs. (A7), (A8), and (A20), we find that

$$v_{iy2} = v_{iz2} = 0. \tag{A22}$$

From Eqs. (A14) and (A17), it follows that

$$v_{ix2} = v_{ex2}. \tag{A23}$$

Substituting Eqs. (A22) and (A23) in Eq. (A6) yields

$$\frac{\partial v_{ex2}}{\partial \xi} - \frac{\partial B_{z1}}{\partial \tau} - \frac{1}{2}\frac{\partial B_{z1}^2}{\partial \xi} + E_{x2} = 0. \tag{A24}$$

Eliminating the lowest-order electron velocities with the aid of Eqs. (A17)–(A19), one finds from Eq. (A9) that

$$E_{x2} + v_{ey2} + \frac{1}{2}\frac{\partial B_{z1}^2}{\partial \xi} = 0, \tag{A25}$$

and from Eq. (A10) that

$$E_{y2} - \left(1 - \frac{\cos^2\theta}{\eta^2}\right)\frac{\partial^2 B_{z1}}{\partial \xi^2} - v_{ex2} - B_{z1}^2 = 0. \tag{A26}$$

Combining the second-lowest order equations of Eqs. (A13) and (A15), and eliminating $n_{j1}$, $v_{jy1}$, and $v_{iy2}$ with the help of Eqs. (A17), (A18), (A20), and (A22), we obtain

$$\frac{\partial B_{z1}}{\partial \tau} - v_{ey2} + \frac{\partial E_{y2}}{\partial \xi} - \frac{1}{2}\frac{\partial B_{z1}^2}{\partial \xi} = 0. \tag{A27}$$

We differentiate Eq. (A26) with respect to $\xi$. Then, by virtue of Eqs. (A25) and (A27), it becomes

$$\left(1 - \frac{\cos^2\theta}{\eta^2}\right)\frac{\partial^3 B_{z1}}{\partial \xi^3} + \frac{\partial v_{ex2}}{\partial \xi} + \frac{\partial B_{z1}^2}{\partial \xi} + \frac{\partial B_{z1}}{\partial \tau} + E_{x2} = 0. \tag{A28}$$

Eliminating $E_{x2}$ and $v_{ex2}$ from Eqs. (A24) and (A28), we obtain the KdV equation

$$\frac{\partial B_{z1}}{\partial \tau} + \frac{3}{2}B_{z1}\frac{\partial B_{z1}}{\partial \xi} + \frac{1}{2}\left(1 - \frac{\cos^2\theta}{\eta^2}\right)\frac{\partial^3 B_{z1}}{\partial \xi^3} = 0. \tag{A29}$$

This is expressed as Eq. (27) with unnormalized variables.


[1] H. E. Petschek, in *AAS-NASA Symposium on the Physics of Solar Flares*, edited by W. N. Hess (NASA, Washington, D.C., 1964), pp. 425–437.
[2] D. Biskamp, *Magnetic Reconnection in Plasmas* (Cambridge University Press, Cambridge, 2000).
[3] J. V. Hollweg, Astrophys. J. **277**, 392 (1984).
[4] W. Grossmann and J. Tataronis, Z. Phys. **261**, 217 (1973).
[5] A. Hasegawa and L. Chen, Phys. Rev. Lett. **32**, 454 (1974); **35**, 370 (1975).
[6] N. Bessho and Y. Ohsawa, Phys. Plasmas **6**, 3076 (1999); **9**, 979 (2002).
[7] H. Hasegawa, S. Usami, and Y. Ohsawa, Phys. Plasmas **10**, 3455 (2003); H. Hasegawa, K. Kato, and Y. Ohsawa, *ibid.* **12**, 082306 (2005).
[8] H. Washimi and T. Taniuti, Phys. Rev. Lett. **17**, 996 (1966).
[9] T. Taniuti and C. C. Wei, J. Phys. Soc. Jpn. **24**, 941 (1968).
[10] T. Kakutani, H. Ono, T. Taniuti, and C. C. Wei, J. Phys. Soc. Jpn. **24**, 1159 (1968).
[11] Y. Ohsawa, Phys. Fluids **29**, 1844 (1986); J. Phys. Soc. Jpn. **57**, 929 (1988).
[12] S. Irie and Y. Ohsawa, Phys. Plasmas **10**, 1253 (2003); M. Toida, Y. Ohsawa, and T. Jyounouchi, *ibid.* **2**, 3329 (1995).
[13] S. J. Buchsbaum, Phys. Fluids **3**, 418 (1960).
[14] A. B. Mikhailovskii and A. I. Smolyakov, Zh. Eksp. Teor. Fiz. **88**, 189 (1985); Sov. Phys. JETP **61**, 109 (1985).
[15] S. Boldyrev, Phys. Plasmas **5**, 1315 (1998).
[16] M. Stix, *The Sun* (Springer-Verlag, Berlin, 1989).
[17] T. Gold, Nature (London) **218**, 731 (1968).
[18] P. Goldreich and W. H. Julian, Astrophys. J. **157**, 869 (1969).
[19] P. A. Sturrock, Astrophys. J. **164**, 529 (1971).
[20] S. Shibata, Astrophys. J. **378**, 239 (1991).
[21] P. C. Liewer, A. T. Lin, J. M. Dawson, and M. Z. Caponi, Phys. Fluids **24**, 1364 (1981).
[22] Y. Ohsawa, Phys. Fluids **29**, 2474 (1986).